Eur. Phys. J. D (2020) 74: 28
https://doi.org/10.1140/epjd/e2020-100545-4

THE EUROPEAN PHYSICAL JOURNAL D

Regular Article

Incoherent and coherent extreme ultraviolet emission from boron plasma

Mazhar Iqbal[1], Rashid A. Ganeev[1,2,a], Ganjaboy S. Boltaev[1,3], Vyacheslav V. Kim[1,3], and Ali S. Alnaser[1]

[1] Department of Physics, American University of Sharjah, P.O. Box 26666, Sharjah, UAE
[2] Faculty of Physics, Voronezh State University, 1 University Square, Voronezh 394006, Russia
[3] Faculty of Physics, National University of Uzbekistan, Tashkent 100174, Uzbekistan

Received 30 October 2019 / Received in Final form 15 December 2019
Published online 11 February 2020

Abstract. The search for reliable sources of incoherent and coherent extreme ultraviolet (XUV) radiation in different spectral ranges is an important task in laser physics. Here we report on the incoherent emission of XUV radiation in the region of 6 nm from boron plasma. The optimization of target ablation allowed the generation of XUV emission mainly originated from a single B IV transition ($\lambda = 6.03$ nm). We also demonstrate the generation of the 806 nm radiation harmonics up to the 55th order ($\lambda = 14.6$ nm) and of tunable near infrared radiation (1280–1400 nm) up to the 35th order ($\lambda = 38$ nm), during the propagation of femtosecond pulses through boron plasma. The incoherent and coherent emissions from this target were compared and analyzed considering the influence of ionic transitions on the B IV emission and harmonic efficiency. We present different schemes of laser-plasma interaction (two-color pump of B plasma, generation of tunable harmonics in XUV range, formation of structured extended plasma, ablation of boron nanoparticles, laser-induced breakdown spectroscopy, overheating of boron targets, quasi-phase matching of plasma harmonics, etc.) during the ablation of boron-containing targets.

1 Introduction

The analysis of useful sources of coherent emission in the short-wavelength range ($\lambda < 100$ nm) is pursued through the generation of such radiation in synchrotrons and from the optical harmonics of ultrashort laser pulses during their propagation in low-dense media (gases and plasmas) and their specular reflection from surfaces. High-order harmonic generation (HHG) studies in the low-dense plasma notably improved the understanding of the restricting and amending processes, thus allowing to analyse processes such as resonance enhancement of single harmonic, nanoparticle-induced enhancement of harmonics, quasi-phase matching of the groups of harmonics, etc. [1–30]. Further search for plasma media that is suitable for the frequency conversion of IR laser pulses towards the extreme ultraviolet (XUV) range requires the analysis of the coherent and incoherent properties of such sources.

The analysis of the optical and nonlinear optical properties of laser-produced plasma (LPP) formed on the surface of boron-containing materials can give useful insights about this medium for different applications. Particularly, the studies presented in [31] have shown that the third-order harmonic generation in boron carbide plasma is sensitive to the presence of atoms, molecules, clusters and nanoparticles in the LPP and can be used as a probe of their density. In [32], 500 fs pulses at $\lambda = 308$ nm were focused on a B_4C plate inserted into the vacuum chamber. They have measured the conversion efficiency for the line emission of H- and He-like B ions, as well as in the range of recombination radiation emitted by He-like B ions (4.86, 6.03, and 4.52 nm, respectively). The feasibility of using thin, freely suspended boron films as a target in femtosecond laser-produced plasma experiments was discussed in [33].

To generate XUV radiation in the vicinity of the water window, laser intensities of 10^{15}–10^{16} W cm^{-2} have to be used, though some schemes of dual laser pumping have demonstrated the application of 10^{14} W cm^{-2} intensities from Nd:YAG class lasers to generate the short-wavelength radiation in this region [34]. The studies of boron emission lines in XUV were reported in [35]. They were generated close to solid state density plasmas with a peak temperature of about 190 eV using 200 μJ, sub-10-fs laser pulses with a high pulse contrast. Time integrated XUV spectroscopy was applied to derive the plasma conditions allowing generation of 4.86, 5.27, and 6.03 nm lines from the ablated boron carbide target. The lack of the higher lines indicates that there is no significant contribution from the plasma to the XUV emission and that there was no significant expansion of the plasma during the laser pulse. A boron nitride plasma X-ray source

[a] e-mail: rashid_ganeev@mail.ru

produced by irradiation of 100 mJ Q-switched YAG laser pulses was also analyzed in [36]. A single line emission at 4.86 nm was selected from the BN plasma using carbon foils.

The interest in boron-containing LPPs is not limited only to the plasma emission and the generation of low-order harmonics. Previous studies have shown the advantages of using this plasma for generating coherent emission in XUV region [37]. Earlier studies have shown that LPP can be used as a nonlinear medium for HHG of ultrashort pulses provided that the limiting factors, such as self-phase modulation and phase mismatch induced by the abundance of free electrons in the plasma plumes, are minimized [38,39]. There are plenty of specific features of the incoherent XUV radiation and HHG in plasma plumes, the foremost one is the wide range of plasma characteristics available for varying the conditions of irradiation through the above channels. Finding new plasma media and optimizing the best plasma plumes under different conditions of laser ablation, for efficient coherent and incoherent emission, is a way for further enhancement of radiation in XUV range.

In this paper, we analyze boron plasma as a source of incoherent and coherent radiation in different ranges of XUV. We present a method for forming strong incoherent emission from the boron plasma in the spectral region of 6 nm. The optimization of the target ablation allows the generation of XUV emission mainly originated from a single B IV transition ($\lambda = 6.03$ nm). We also demonstrate generation of the 806 nm radiation harmonics up to the 55th order ($\lambda = 14.6$ nm) and of tunable near infrared radiation (1280–1400 nm) up to the 35th order ($\lambda = 38$ nm) during the propagation of femtosecond pulses through the boron plasma.

2 Experimental arrangements

Ti:sapphire laser was used as the source of uncompressed picosecond pulses for the generation of the LPP on the surface of bulk boron target. The characteristics of this radiation were as follows: central wavelength 806 nm, pulse duration 370 ps, pulse energy up to $E_{\rm hp} = 6$ mJ, 10 Hz pulse repetition rate. We used cylindrical lens ($f = 200$ mm) to form extended LPP with size of 5×0.08 mm^2 using heating pulse of intensity up to $I_{\rm hp} = 4 \times 10^9$ W cm^{-2}. This plasma was used for HHG during propagation of compressed femtosecond driving pulses from the same laser. The parameters of these driving pulses were as follows: pulse duration 35 fs, pulse energy up to $E_{\rm dp} = 1$ mJ, the intensity of the driving pulses at the focus area was varied up to 4×10^{14} W cm^{-2}. The optimal conditions for harmonic generation in boron plasma were found at 50 ns delay between the heating and driving pulses and at a distance of $\sim$150 μm from the target surface. These characteristics of the heating and driving pulses were used for generation of coherent XUV emission through HHG (Fig. 1).

The studies of plasma emission in the deep XUV range were performed using 370 ps heating pulses of variable intensity on the target surface in the range of

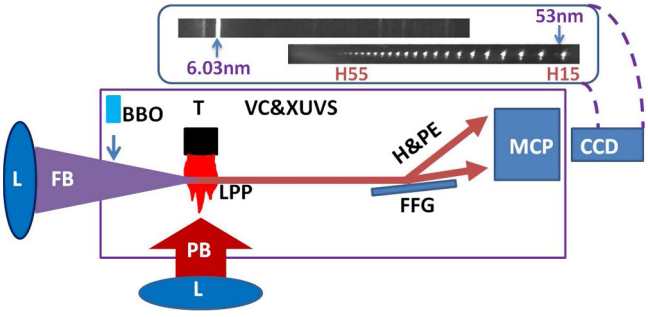

Fig. 1. Experimental scheme for the studies of incoherent and coherent emission from the boron plasma. L, focusing lenses for driving and heating pulses; BBO, boron borate crystal; T, boron target; FB, driving femtosecond beam; PB, heating picosecond beam; LPP, laser-produced plasma formed on the surface of boron target; VC & XUVS, vacuum chamber and extreme ultraviolet spectrometer; H & PE, harmonic and plasma emission; FFG, flat field grating; MCP, microchannel plate; CCD, charge-coupled device camera. Inset: images of plasma and harmonic spectra. Upper panel shows the strong incoherent emission of B IV line (6.03 nm) prevailing over other plasma emission components in the XUV range of 2–30 nm. Bottom panel demonstrates the coherent emission spectrum arising from the process of HHG in boron LPP. Harmonic orders between H15 ($\lambda = 53$ nm) and H55 ($\lambda = 14.5$ nm) are shown.

1×10^{10} W cm^{-2} to 3×10^{10} W cm^{-2}. The laser plasma was also formed using nanosecond pulses from Nd:YAG laser. We also applied the optical parametric oscillator to produce the femtosecond tunable IR pulses ($t = 70$ fs, $E = 1.2$ mJ) in the range of 1100–1600 nm, which were used as the driving pulses for HHG. The plasma and harmonic emissions were analyzed using XUV spectrometer.

As mentioned earlier, laser plasma was formed using picosecond or nanosecond pulses. The latter pulses were used to probe the dynamics of plasma spreading and the formation of the optimum cloud of particles at the moment the femtosecond driving pulses propagate nearby the target surface. We used a scheme of heating nanosecond pulses and driving femtosecond pulses from different laser sources for HHG in plasmas. The ablation of boron-contained targets was carried out by 5 ns, 1064 nm, 10 Hz pulses. An electronic delay between nanosecond and femtosecond pulses allowed applying sufficiently longer delays between two pulses compared with the optical delay technique. The delay between pulses was synchronized and tuned using the delay generator. The synchronization of two laser sources allows analyzing the enhancement of harmonics in different groups of atomic or molecular particles produced during the ablation of bulk materials, or targets initially contain multi-atomic species. The main advantage of this approach is the control of the delay between the heating nanosecond pulses and the driving femtosecond pulses over a wide range between 0 and 10^5 ns, which is sufficient to analyze fast and slow components of ablating material spreading out from the target. The use of the low-pulse repetition rate nanosecond Nd:YAG lasers as the sources of heating pulses may also offer some additional

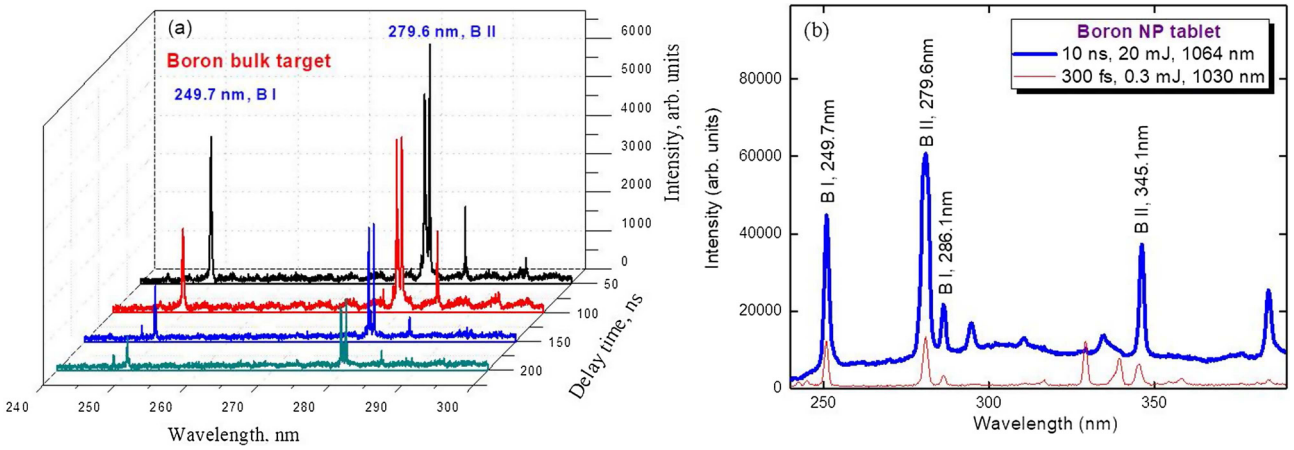

Fig. 2. (a) Dynamics of plasma emission spectrum in UV range (200–300 nm) during ablation of bulk boron target by 10 ns, 1064 nm pulses. (b) Time-integrated spectra of plasma emission from boron NP tablet in the case of ablation by 300 fs (thin red curve) and 10 ns (thick blue curve) pulses.

advantages compared with the commonly used picosecond pulses of the same repetition rate and wavelength. The application of nanosecond pulses to ablate the surface of targets allows the formation of less ionized and less excited plasma during longer periods of laser-matter interaction compared with picosecond pulses. This conclusion is based on the analysis of the nanosecond and picosecond ablation-induced plasma emission in the visible and extreme ultraviolet ranges in the case of formation of the optimal plasmas leading to generation of the highest harmonic yields. Different delays between heating and driving pulses from 5 to 1000 ns were employed in the present experiments, with the highest harmonic yield obtained at ∼90 ns delay. The harmonic yield at the delays larger than 600 ns was notably decreased due to removal of the largest part of plasma cloud out from the path of the driving beam propagated at the 150 μm distance above the target surface.

To produce multijet plasmas (MJP), multislit mask (MSM) was installed between the cylindrical lens and the Boron target. We analyzed the application of three MSMs with different slit sizes, two with 0.2 and 0.5 mm slits equidistantly-spaced from each other, and one with slit size of 0.3 mm separated by 0.8 mm shield between the slits. The plasma formation was accomplished 38 and 75 ns prior to propagation of the femtosecond pulses through the MJP. These delays between the heating and driving pulses were chosen to analyze different properties of the quasi-phase matching (QPM) between the interacting and generating waves. The maximal used intensity of 800 nm pulses in the plasma area was 5×10^{14} W cm^{-2}. This radiation propagated through imperforated plasma or MJP 75 ns after ablating the targets by picosecond pulses.

The size of the bulk boron target was $5 \times 5 \times 2$ mm^3 (purity 99.6%, Sigma-Aldrich). The B target was mounted on a three-coordinate holder placed inside a vacuum chamber (∼10^{-5} mbar) to adjust with respect to the propagating femtosecond pulse. We also ablated tablets that were prepared by pressing the boron nanoparticle (NP) powder. The mean size of NPs was 120 nm (purity: 99.9%, bulk density: 1.6–1.8 g/cm^3, morphology: spherical particles, appearance: black powder). The diameter of tablets was 5 mm. In addition, we formed boron NP-contained targets by gluing NPs on the glass substrates. No XUV emission and harmonic generation was observed in the case of ablation of pure dried glue.

3 Incoherent emission of boron plasma at $\lambda = 6.03$ nm

The formation of plasma plume should satisfy some specific requirements, which can be essential for efficient application of such LPP for different tasks. Particularly, as it was shown above, the "optimal" conditions of target ablation allowed the generation of strong 6.03 nm emission, while other emission lines become suppressed. The application of LPP for HHG also requires the specific conditions of plasma formation. The over-dense plasmas generated during strong ablation may strongly suppress the efficiency of high-order harmonics due to the destructive influence of the free electrons appearing at these conditions (see also Sect. 4). Previous studies have shown that the "optimal" plasma for HHG is the one which does not demonstrate strong emission [11,12,14,21]. In that case one can expect the fulfillment of the phase matching conditions for as much as possible harmonic orders. In this connection, one can determine the suitable conditions for LPP formation using the analysis of the plasma emission in the visible and UV ranges during ablation of targets in ambient conditions in the presence of air.

The dynamics of the plasma emission spectrum in the UV range (200–300 nm) during ablation of bulk boron target by 10 ns, 1064 nm pulses are shown in Figure 2a. The emission lines in the UV region were analyzed using laser-induced breakdown spectroscopy (LIBS) during 1000 ns from the beginning of ablation, with the step of 50 ns. The fluence of heating radiation was chosen to be optimal for the 6.03 nm emission being generated at vacuum

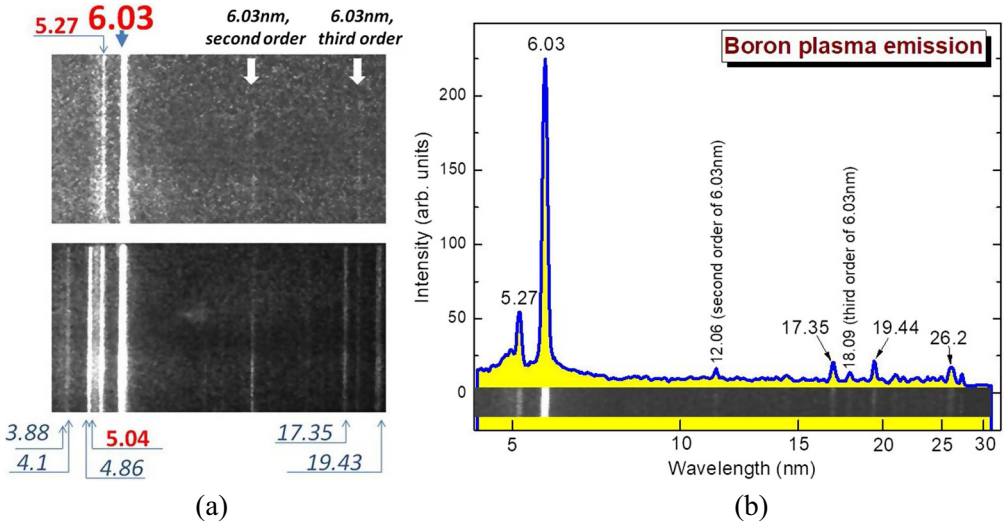

Fig. 3. (a) Images of plasma emission from ablated bulk boron target using the 200 ps heating pulses of different fluence (upper panel: 2 J cm^{-2}; bottom panel: 6 J cm^{-2}). (b) Intensity distribution of B NPs plasma emission in the case of ablation by 50 fs pulses.

conditions. One can see the decay of most intense lines in this spectral range [249.7 (B I) and 279.6 (B II) nm], which then almost disappeared after 500 ns (not shown in the picture). The application of time-resolved LIBS for the determination of the best conditions of ablation may be useful for different tasks, like short-wavelength plasma emission, HHG, LIBS characterization, laser ablation deposition, etc.

We also analyzed the comparative time-integrated UV spectra of ablated boron NP tablet using the 10 ns and 300 fs heating pulses (Fig. 2b). Application of longer pulses led to formation of the continuum emission alongside the emission from the B I and B II particles. Femtosecond heating pulses caused the emission of neutral and singly charged boron particles without the continuum component.

Prior to the XUV studies of boron plasma we analyzed the emission from different ablated materials. Plasma emission from different ablating targets demonstrated a notable difference in the intensities of deep XUV (i.e. in the range of >15 nm). In this regard, boron plasma can provide strongly distinguished emission in the 4.9–6.0 nm range, without the notable emission in other ranges of shorter-wavelength part of XUV using the specially chosen pulse duration and fluence of the heating radiation. Our experiments with other metal targets did not show such difference in the emission lines in the shortest wavelength range of XUV.

Figure 3a shows two images of plasma emission from ablated solid boron target in the case of ablation by 370 ps heating pulses of different fluence. In these spectra, the B V (B Ly$_\alpha$, 4.86 nm), B IV (B He$_\alpha$, 6.03 nm), and B IV (B He$_\beta$, 5.27 nm) lines are identified. The upper panel shows that there are only two emission lines from B IV ions (6.03 nm, 2p-1s, and 5.27 nm, 3p-1s), which dominate in the XUV range of 3–20 nm. Two other weak lines (12.06 and 18.09 nm) shown by arrows correspond to the second and third orders of diffraction from the 2400 grooves/mm flat field grating of XUV spectrometer. This spectrum was obtained during ablation of bulk target by picosecond pulses at a moderate fluence (2 J cm^{-2}). The increase of the fluence of the heating pulses up to 6 J cm^{-2} (Fig. 3a, bottom image) led to further increase of the intensity of 6.03 nm emission. Alongside the increase of this emission, the spectral lines from B V shown by italic letters (3.88, 4.1, 4.86, 17.35, 19.43 nm) appeared in these spectra, though their intensities, except of 4.86 nm line, were incomparable with the B IV emission.

We also ablated the boron NP tablet by the same fluence of femtosecond pulses as in the latter case. Plasma emission from B IV at $\lambda = 6.03$ nm was 10–20 times stronger than other emission lines from B V ions (Fig. 3b). We used 50 fs, 800 nm pulses at the fluence of 1 J cm^{-2} on the NP tablet surface. The ablation of NPs by smaller fluence of heating radiation compared with the case of picosecond pulses led to even larger ratio between the B IV emission and other emission lines. Similar features were observed in the case of ablation of the glued boron NPs.

We carried out the quantitative comparison of 6.03 nm emission during the ablation of bulk boron target and B NPs-contained target at similar experimental conditions (fluence, pulse duration and energy, focusing conditions). The emission from the NP target was 3–5 times stronger compared to the ablation of the bulk target. The main obstacle in using these efficient NP-based sources of strong B IV emission ($\lambda = 6.03$ nm) is the difficulty in maintaining the stability of this emission due to the degradation of NP-contained target. The rotation of NP target may, to some extent, diminish this problem.

Due to the high pulse intensities, incoherent short-wavelength radiation can be generated if laser radiation interacts with solid and nanostructured matter. In cases of those materials processing, the emission rate decisively depends on the laser parameters and the physical

properties of the target material. The interaction of intense short pulse laser with atomic clusters [40,41] has become an important area of research. The main characteristic of these small sized species is the near solid density inside them that results in an enhanced absorption of laser energy via collisional processes and consequently in an increase of X-ray conversion efficiency. A theoretical model of strong soft X-ray emission from laser irradiated clusters was developed in [42]. In this model, an intense short pulse laser of Gaussian radial and temporal profiles impinged on a clustered target, heats the cluster electrons and leads to Bremsstrahlung emission of X-rays. As the clusters expand under hydrodynamic pressure, plasma frequency of the cluster electrons decreases. It has been suggested that the strong light-NP interaction can cause the efficient blast of clusters leading to strong emission covering the 1–10 nm spectral region. The larger efficiency of these sources can be attributed to the confinement of larger portion of heating light in a small area, which causes the transfer of this energy into the energy of short-wavelength photons.

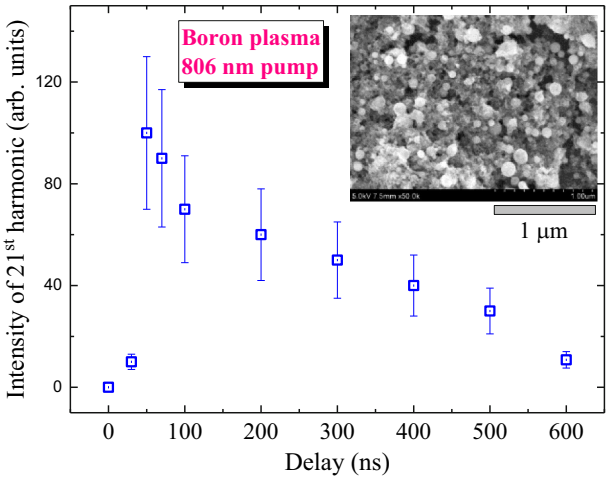

Fig. 4. Variation of H21 generated in boron plasma at different delays between the heating 5 ns pulse and driving 35 fs pulse. Inset shows the SEM image of deposited debris from ablated bulk boron.

4 HHG in boron plasma

4.1 Characterization of plasma for efficient HHG

The analysis of plasma dynamics was carried out by studying the delay dependence of the harmonic yield from the B plasma. For these purposes we used the nanosecond pulses for plasma formation. The radiation of Ti:sapphire laser ($\lambda = 806$ nm, $\tau = 35$ fs) was used for the interaction with the plasma produced by Nd:YAG laser ($\lambda = 1064$ nm, $\tau = 5$ ns) to generate the high-order harmonics. The use of a light target such as B ($Z = 5$) allows maximal yield of HHG at a short delay between the heating pulses producing LPP and the driving femtosecond pulses propagating through the different stages of spreading plasma, prior to the interaction of bulk amount of the ablated material with the driving beam.

Figure 4 shows the dynamics of boron plasma formation and spreading along a broad range of delays between the heating nanosecond pulses and driving femtosecond pulses. Here we show that the optimization of high-order harmonic yield strongly depends on the delay between the heating and driving lasers. The maximal harmonic yield in our case was observed at 50 ns from the beginning of ablation.

The novelty in the present work stems from using nanostructured targets and nanosecond heating pulses, which allowed achieving the highest yield of harmonic emission from the boron plasma in different spectral ranges. Firstly, harmonics from B plasma have been obtained earlier using ablation by picosecond pulses [37,43,44]. Secondly, the targets, which were used in previous studies, comprised from species in the bulk state. The combination of nanostructured targets and nanosecond heating produced the highest harmonic yield for the conditions of present studies. Our analysis of the components of plasma ablation was carried out by studying the debris deposited on a nearby silicon substrate during ablation of bulk boron and B NPs. Deposited B NPs were observed in the case of B NP tablet ablation, as well as during ablation of bulk target (see the insets in Figs. 4 and 6). Optimal fluencies for ablation of boron bulk target, boron NPs tablet, and glued boron NPs were chosen by achieving strongest harmonic yield.

The quantitative determination of plasma concentration is yet resolved properly, though different methods were offered to determine this parameter. One has to determine the concentration of particles at the moment of the driving pulse propagation leading to the highest harmonic conversion efficiency. Obviously the pressure of particles initially grows from zero level and then gradually decreases. We did not carry out the measurements of the dynamics of plasma concentration but rather estimated it based on the principles developed earlier in [45] for the laser ablation of solids. Regarding the plasma concentration, one has to determine (or at least, estimate) the concentration of neutrals, ions and electrons to define their influence on the process of HHG. To understand this phenomenon, the simulations using the hydrodynamic code HYADES have been reported [46]. The expansion of a silver slab interacting with a laser pulse was simulated and then the electron density, ionization level, and ion density were determined as the functions of the heating pulse intensity at a fixed distance from the target surface.

Another approach for determining the plasma characteristics from the ablation of carbon, at the conditions that led to largest harmonic yield, was reported in [47]. A three-dimensional molecular dynamical simulation of laser ablation of graphite was performed using the molecular dynamics code ITAP IMD [48]. In those studies, the concentrations of carbon plasma were calculated under the experimental conditions of target ablation allowing efficient harmonic generation. The corresponding concentrations were found to be exceeding 10^{17} cm^{-3} in the case of ablation by 8 ps pulses. Notice that the concentrations of plasma particles above the graphite target surface in the area of the femtosecond pulse propagation were calculated to vary between 1.1×10^{17} and 4×10^{17} cm^{-3} depending on

the conditions of optimal HHG at two different energies and fluencies of heating pulses. This difference highlights the important role of the pulse energy, which is responsible for the difference in the concentrations of the plasma plumes.

Obviously, the difference in the experimental arrangements makes it difficult to determine with high accuracy the plasma concentration, as well as the partial ratio of its components, in another set of experiments. Meanwhile, the similarity in the dynamics of HHG variations with the delay between heating and driving pulses, fluence of heating pulses, distance from target, etc. may lead to the conclusion on the approximate similarity of the plasma characteristics at the conditions of the maximal harmonic yield. Based on the above assumptions and taking into account the studies reported in [46,47], we concluded about the estimations of the plasma characterization in the case of ablated solid boron at the moment of propagation of our driving beam through the plasma cloud at the conditions of highest HHG efficiency ($2 \times 10^{17}\,\mathrm{cm}^{-3}$).

Meanwhile, no estimates are available for the case of ablated powdered materials. Different absorbance characteristics, uncertainty in the distribution of absorbed heat among the NPs, difference of their thermodynamic characteristics (i.e. melting and evaporation) with regard to the solid boron, and other peculiarities did not allow determining the concentration of NPs at the moment of the driving beam propagation.

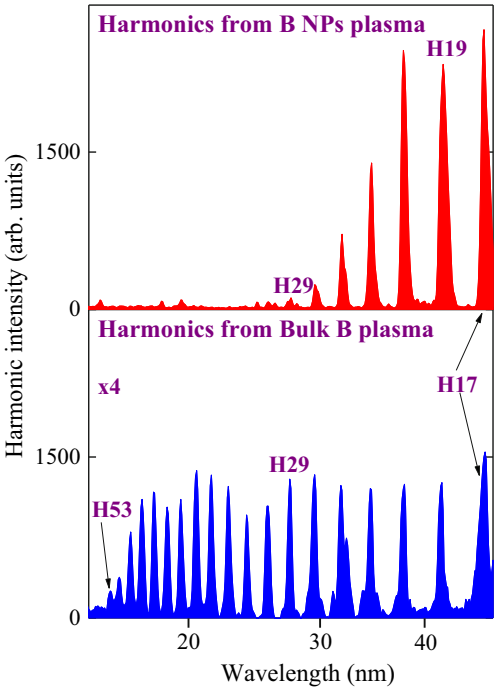

Fig. 5. Comparison of lower- and higher-order harmonics generated in the NP-contained plasma (upper panel) and the plasma produced on the bulk boron target (bottom panel). Bottom spectrum was magnified with a factor of four for comparison with upper spectrum.

4.2 Analysis of harmonic cutoffs from different plasma consistencies

We observed different cutoffs in the case of bulk (fifties orders) and nanopowder (twenties orders) boron targets. The former results were reported in earlier studies of ablated bulk boron targets [37,43], while the lower orders of harmonics from the nanoparticle-contained plasmas became a frequently reported feature once the comparison of two LPP media (i.e. those contained mono-particles and multi-particles of the same elemental consistence) was discussed earlier (see for example [49]).

Figure 5 shows that lower-order harmonics from NP plasma were approximately eight times stronger compared to those produced from monomer-containing plasma. The ablation conditions with respect to pulse energy and fluence of the ablation pulse as well as of the driving fundamental pulse remained identical for these two samples. The same holds for the other experimental parameters, like the distance between the target surface and the driving beam, the pulse duration of the ablation pulses, and the delay between the ablation and driving pulses. The intensity ratio strongly decreases for higher harmonics, until at the 29th order the harmonic from the nanoparticle target shows an intensity of only 3% of that at the 17th harmonic and becomes smaller by a factor of five compared to the B bulk harmonic.

The harmonics generated from the nanoparticle plasma target showed a larger divergence than those from the bulk target. The observation of only relatively low-order harmonics from the B nanoparticle containing plasma could be related to the origin of nanoparticle-induced HHG, which is assumed to occur from neutral particles. Meanwhile, the higher-order harmonics from ablated bulk boron target were attributed to the involvement of singly charged ions in the HHG.

The plasma produced on the bulk boron target allowed generation of the harmonics above the fifties orders. The other two plasmas showed lower harmonic cut-offs (H25 and H21 in the case of B NP tablet and glued B NPs, respectively), while the intensities of the harmonics in the plateau region were notably stronger compared with those generated from the ablated bulk boron target. The comparison of these plasma formations, from the point of view of the stability of harmonic emission, showed that plasma formed on the bulk target was the best choice among the three ablated species. The most probable reason for the difference of harmonic emission from the ablated bulk boron and the two other targets is the difference in the constituencies of plasmas in these three cases at the optimal conditions of laser ablation. Probably, the neutral atoms of boron play important role in harmonic generation from NP-containing plasmas. Correspondingly, their involvement in HHG may explain the low harmonic cut-off observed in the case of these plasmas. Similarly, the lower conversion efficiency in bulk B ablation compared with two boron NP plasmas could be also explained by the preferable involvement of ions in harmonic generation in the former case, while, in the case of ablated NP targets, one can expect the appearance of the boron clusters alongside the NPs, which may enhance the harmonic emission [11,13].

When comparing harmonics from NP and bulk targets, an essential parameter that needs to be taken into account is the heating pulse intensity. The heating pulse intensity cannot be maintained similar for three targets used in these experiments. The comparison of harmonic yields was provided at the best conditions of the bulk boron plasma and NP boron plasma formation. In the case of 370 ps heating pulses the intensity $I_{hp} = 4 \times 10^9\,\mathrm{W\,cm^{-2}}$ was maintained along the whole extended bulk target. This intensity corresponded to $1.5\,\mathrm{J\,cm^{-2}}$ fluence. Previous studies of HHG in different plasmas have shown that the fluence rather than intensity of heating pulses is the most relevant parameter that defines the best conditions of plasma formation. Particularly, the comparative studies were carried out in [50] on the plasma formation using pulses of different duration (12 ps and 40 fs). Note that in these two cases approximately the same optimal fluence of the heating pulses was determined ($\sim 1\,\mathrm{J\,cm^{-2}}$) by using the same focusing conditions and heating pulse energy, while the intensities of the heating 12 ps and 40 fs pulses were $9 \times 10^{10}\,\mathrm{W\,cm^{-2}}$ and $2.5 \times 10^{13}\,\mathrm{W\,cm^{-2}}$, respectively.

One of the main goals of our present studies was to define which parameter, fluence or intensity of the heating pulse, plays the dominant role in the formation of suitable plasma for efficient HHG. Our HHG experiments using 5 ns heating pulses also determined the optimal fluence ($\sim 8\,\mathrm{J\,cm^{-2}}$) of the same order on the bulk boron target at which the maximal harmonic yield was achieved, while the intensity of these pulses on the ablating surface ($\sim 1.5 \times 10^9\,\mathrm{W\,cm^{-2}}$) was notably smaller with regard to the case of ablation by 370 ps pulses.

4.3 Two-color pump and quasi-phase matching studies

Previous studies have shown that enhanced harmonics can be achieved at the QPM conditions of generating coherent XUV photons once multi-jet LPP are used instead of extended imperforated plasma formations [51–54], which is similar to earlier reported achievements in QPM using gas multi-jet gas targets [55–58]. The QPM during ablation of targets is based on the division of extended plasma into a set of equidistantly separated plasma jets by inserting the MSM in front of the ablating surface or by using the perforated targets.

This mechanism is useful for producing efficient sources of short-wavelength ultra-short pulses for various applications and studies of the properties of harmonic emitters. The dephasing between the propagating harmonic wave and laser-induced polarization is mainly caused by the dispersion of the medium and becomes essential in the presence of a significant number of free electrons. Due to the difference in the velocity of the waves, at some distance from the beginning of the medium, the phase shift becomes close to π. Beyond this distance, called the coherence length, the constructive accumulation of harmonic photons is reversed and the harmonic energy starts to decrease. The implementation of this concept for the case of plasma harmonics widely broadens the field of studies due to the overwhelming prevalence of the ablated solid species used in the latter case over a few gases routinely exploited in conventional HHG. One also should note that the gases used in HHG at QPM conditions are usually denser than LPP ($\sim 10^{18}$ and $\sim 10^{17}\,\mathrm{cm^{-3}}$ respectively), which can restrict conversion of plateau harmonics due to absorption in noble gases, while for plasmas absorption is insignificant. In the meantime, the formation of QPM conditions in the laser plasmas containing free electrons is more complicated due to low concentration of plasma for intensity-based optimization and general problems related to precise control of concentration of ions and electrons in the interaction region.

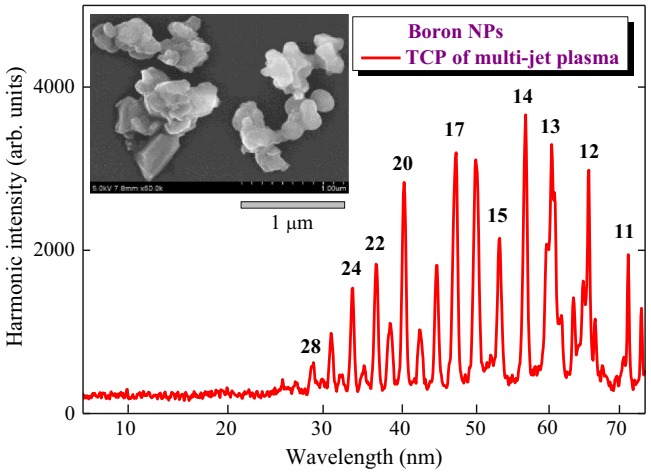

Fig. 6. Two-color pump of multi-jet boron plasma. Inset shows the SEM image of deposited debris from ablated NPs.

Two-color pump (TCP) scheme can be used to further improve the HHG yield. The commonly used way is the application of Ti:sapphire laser and its second-order harmonic (H2) leading to doubling the number of generated harmonics from odd orders, in the case of single-color pump (SCP), to odd and even orders, in the case of TCP. TCP with gases and plasmas targets allowed the analysis of various microscopic and macroscopic effects and polarization-related processes [43,59,60]. In the present studies, we used the TCP scheme comprising 806 nm pulses and its second harmonic radiation (403 nm). The 0.5-mm-thick boron borate crystal (BBO, type I, $O = 21°$) was installed inside the vacuum chamber on the path of the focused driving pulse (Fig. 1). The conversion efficiency of H2 pulses was 4%. In these studies, we used the MJPs produced by installing the multi-slit mask in front of the extended target to analyze the role of quasi-phase matching in different ranges of XUV spectrum. This target was irradiated by the heating pulse focused using a cylindrical lens. The MJP configuration was comprised of 12 plasma jets with the sizes of 0.2 mm each.

Figure 6 shows the TCP-induced harmonic spectrum from the plasma produced on B NPs pressed tablet. Though the ratio of second field (403 nm) compared with fundamental field was notably small (1:25), the application of TCP allowed the four-fold growth of the conversion efficiency of odd harmonics compared with the case of SCP. We also achieved the stronger even harmonics compared with the odd ones. Meanwhile, in the case of TCP we did not observe the enhancement of the group of

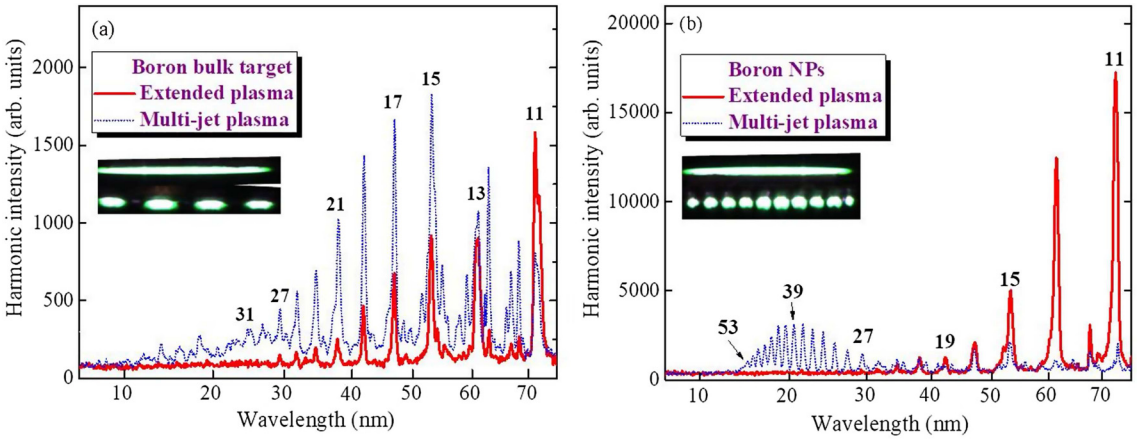

Fig. 7. (a) Harmonic spectra from ablated bulk boron using the extended (solid curve) and multi-jet (dotted curve) plasmas. Inset: images of extended and 4-jet plasmas. (b) The same in the case of the ablation of B NP-contained tablet. Inset: images of extended and 10-jet plasmas.

harmonics for which the quasi-phase matching conditions were fulfilled (Fig. 6).

Another pattern of harmonic spectrum from MJP was obtained in the case of SCP of boron plasma (Fig. 7a, dotted curve). In that case the plasma contained four 0.5 mm long jets. One can see that the shorter wavelength harmonics became stronger compared to the case of extended homogeneous plasma produced on the boron bulk target (Fig. 7a, solid curve).

We were able to further modify the harmonic distribution from the multi-jet plasma by using the 10-jet plasma produced during B NP ablation. In the case of extended homogeneous plasma produced by picosecond pulses on the B NP pressed tablet, we observed the ordinary decrease of harmonics up to H25 (Fig. 7b, solid curve). The formation of multi-jet plasma using the multi-slit mask containing 0.2 mm slits led to drastic change in the harmonic distribution (Fig. 7b, dotted curve). The group of enhanced harmonics centered at around of H39 dominated the HHG spectrum, while the lower-order harmonics were suppressed.

The mechanism of this group of harmonics enhancement is well understood and determined by the coherent addition of the harmonic yield in each plasma jet at the conditions of coincidence of the coherence length of harmonic and the sizes of jet. The present studies show the applicability of this approach for the NP-containing plasmas. We studied the comparison of HHG in boron-containing plasmas using different SCP and TCP schemes. The lower conversion efficiency in bulk B plasma compared with B NP plasmas could be explained by efficient participation of B clusters in HHG, contrary to the atoms and ions of boron. Similar conclusion was drawn during lower-order harmonic generation studies of the plasmas produced by femtosecond and picosecond pulses [61,62]. Thus the most probable reason in the difference of harmonic emission properties of bulk B and two B NP ablated targets is the difference in the constituencies of plasmas in these three cases.

The steep decrease of the intensity of low-order harmonics was followed by a plateau pattern. The harmonic conversion efficiency was estimated by considering the typical conversion efficiency from carbon plasma (8×10^{-6} [63]). Similar or even higher values of this parameter were reported by different groups studying carbon plasma as the efficient medium for harmonics generation [11,47,64]. We compared the conversion efficiencies from boron and carbon plasmas. From this comparison, we deduced the ratio between the HHG conversion efficiencies in the plateau range of harmonics distribution in these two cases and correspondingly determined the conversion efficiency in the case of ablation of the bulk boron target. The conversion efficiencies were measured to be between 2×10^{-4} (for third harmonic) to 10^{-7} (along the plateau region).

The HHG appeared to be efficient in the case of neutral and singly ionized plasma when the multiple charged ion and electron concentrations were negligible. We also observed that the coincidence of harmonics and plasma emission wavelengths does not lead to the enhancement or decrease of the conversion efficiency of these harmonic. The process of harmonic enhancement in the vicinity of some ionic lines requires the strong oscillator strength of the involved transitions, as well as the fulfillment of the suitable phase matching conditions between the driving and harmonic waves. Meanwhile, being earlier demonstrated only in a few LPPs (In, Mn, Cr, Sn), this process was not observed in the present studies in the case of boron plasma (Fig. 8a). One can see the coincidence or closeness of H11 and H15 with the strong emission lines of boron, which did not cause the enhancement of those harmonics.

The spectral tuning of driving radiation was carried out using the optical parametric amplifier pumped by 800 nm laser. This radiation was tuned between 1100 and 1600 nm. Figure 8b shows the tuning of harmonic spectra along the strong ionic lines of boron (67.7 and 72.5 nm, see upper panel) using the TCP configuration. No influence of strong B III transition (67.7 nm) on the tunable H20 was observed, similarly to the absence of the enhancement of H18 tuned along the strong B IV transition (72.5 nm). All spectra of generated coherent radiation represented a plateau-like distribution of harmonics.

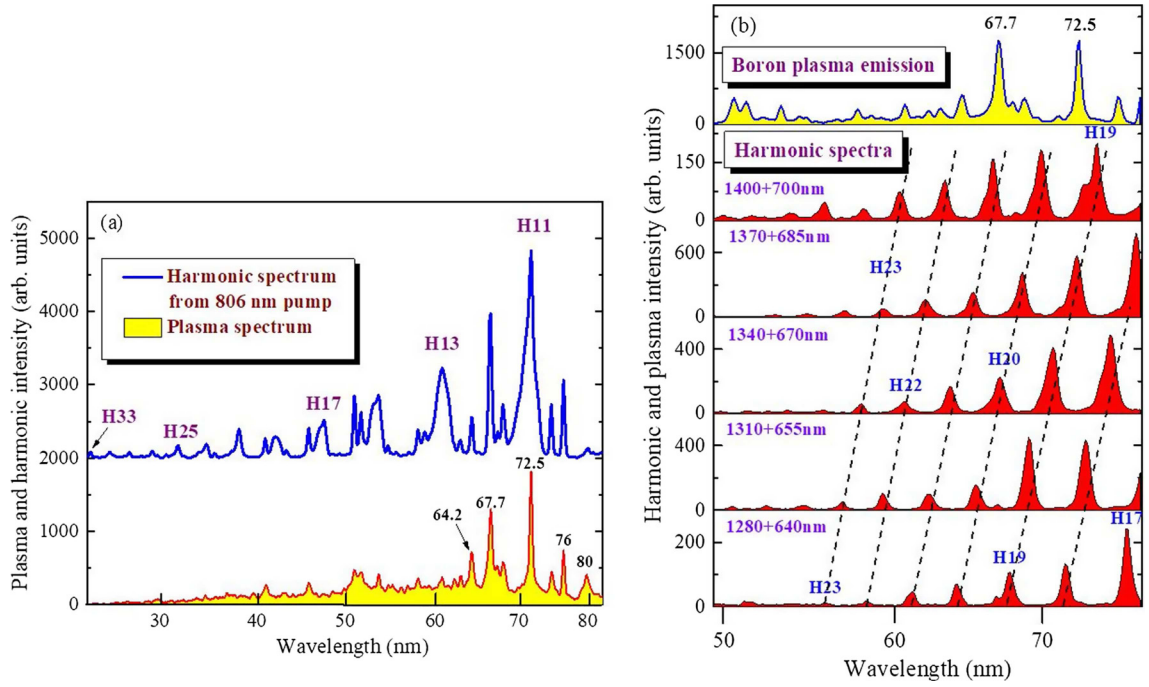

Fig. 8. (a) Harmonic spectrum along with some plasma emission lines from bulk boron at optimal conditions of ablation leading to maximal harmonic yield (upper panel) and plasma emission spectrum at stronger irradiation of target, without the propagation of driving pulses through LPP (bottom panel). (b) Plasma emission (upper panel) and harmonic spectra (other panels) using tunable near infrared radiation (1280–1400 nm) and its second harmonic from the optical parametric oscillator.

The first ever observation of a plateau in the high-order harmonics generated by an ablation plume at a solid surface, was reported in reference [37]. Boron plasma has accidentally demonstrated advanced properties as a medium that demonstrates the harmonic orders far exceeding those reported in previous studies. Further optimization of this process was reported in [43]. The analysis of the harmonics generation from low-excited boron plasma was presented in the case when the confocal parameter of the focused radiation was close to the plasma sizes (1.2 and 0.6 mm, respectively). The motivation of these studies was to reveal the restricting factors for the conversion efficiency and cutoff energy. The conversion efficiencies for the low- and high-order harmonics reported in [44] focused on the longitudinal arrangement of heating and driving pulses propagation through the hole in the boron target, while our present studies employ orthogonal scheme of two pulses.

New relevant knowledge of these studies is related to the application of suitable ablating material using the optimized experimental conditions of plasma formation, which allows the generation of either stable high-order harmonics or strong incoherent emission in the short-wavelength range of XUV. This knowledge is applicable for the practical use of the plasma emission and HHG technique, as well as for the fundamental understanding of the harmonic and incoherent emission generation in the plasmas. Our analysis of the components of plasma ablation was carried out by studying the debris deposited on the nearby silicon substrate during ablation of bulk boron and B NPs. Deposited B NPs were observed in the case of B NP tablet ablation, as well as during ablation of bulk target. Optimal fluencies for ablation of boron bulk target, boron NPs tablet, and glued boron NPs were chosen by achieving strongest harmonic yield.

5 Conclusions

We have shown the strong incoherent emission from boron plasma at ∼6 nm and coherent emission in the 15–53 nm spectral range. In the presented HHG studies, we have demonstrated the generation of the 806 nm radiation harmonics up to the 55th order ($\lambda = 14.6$ nm) and of tunable near infrared radiation (1280–1400 nm) up to the 35th order ($\lambda = 38$ nm) during the propagation of femtosecond pulses through the boron plasma. The incoherent and coherent emissions from this target were compared and analyzed from considering the influence of ionic transitions on the harmonic conversion efficiency. We have presented different schemes of laser-plasma interaction (two-color pump of B plasma, generation of tunable harmonics in XUV range, formation of structured extended plasma, application of boron nanoparticles, laser-induced breakdown spectroscopy, overheating of boron targets, quasi-phase matching of plasma harmonics, etc.) and we found major characteristics that would prevail during laser ablation and HHG. In our particular case (i.e. the plasma produced on the three boron-containing targets) we compared three characteristics: (a) stability of harmonic emission, (b) extension of harmonic cutoff, and (c) harmonic yield. The plasma produced on bulk boron can be considered

as the best choice among the three ablated targets when it comes to harmonic emission stability and cut off extension. On the other hand the B NP plasma showed the best characteristics to produced highest yield. The fluencies of heating pulses for the HHG experiments were found different from those used in the plasma emission studies. In each case we had chosen the "optimal" fluence of heating pulses. This term refers to the maximal efficiency of harmonic generation or incoherent emission in the studied plasmas plumes. Furthermore, we found that the conditions of efficient emission of 6 nm radiation from the overionized plasma were unsuitable for efficient HHG. We have analyzed the plasma during ablation of boron-containing targets and found the optimal conditions allowing generation of almost single emission line ($\lambda = 6.03$ nm, B IV) in the 2–20 nm spectral range.

Author contribution statement

M. Iqbal, R.A. Ganeev, G.S. Boltaev, and V.V. Kim performed the investigation of the coherent extreme ultraviolet emission from boron plasma. R.A. Ganeev studied the incoherent emission of the boron laser-produced plasma. The writing, reviewing and editing of manuscript were performed by R.A. Ganeev and A.S. Alnaser.

References

1. R.A. Ganeev, H. Singhal, P.A. Naik, U. Chakravarty, V. Arora, J.A. Chakera, R.A. Khan, M. Raghuramaiah, S.R. Kumbhare, R.P. Kushwaha, P.D. Gupta, Appl. Phys. B **87**, 243 (2007)
2. T. Ozaki, L.B. Elouga Bom, R. Ganeev, J.-C. Kieffer, M. Suzuki, H. Kuroda, Laser Part. Beams **25**, 321 (2007)
3. R.A. Ganeev, M. Suzuki, M. Baba, H. Kuroda, Phys. Rev. A **76**, 023805 (2007)
4. L.B. Elouga Bom, F. Bouzid, F. Vidal, J.C. Kieffer, T. Ozaki, J. Phys. B: At. Mol. Opt. Phys. **41**, 215401 (2008)
5. H. Singhal, V. Arora, B.S. Rao, P.A. Naik, U. Chakravarty, R.A. Khan, P.D. Gupta, Phys. Rev. A **79**, 023807 (2009)
6. I.A. Kulagin, T. Usmanov, Opt. Lett. **34**, 2616 (2009)
7. D. Cricchio, P.P. Corso, E. Fiordilino, G. Orlando, F. Persico, J. Phys. B **42**, 085404 (2009)
8. V. Strelkov, Phys. Rev. Lett. **104**, 123901 (2010)
9. D.B. Milošević, Phys. Rev. A **81**, 023802 (2010)
10. M.V. Frolov, N.L. Manakov, A.F. Starace, Phys. Rev. A **82**, 023424 (2010)
11. L.B. Elouga Bom, Y. Pertot, V.R. Bhardwaj, T. Ozaki, Opt. Express **19**, 3077 (2011)
12. R.A. Ganeev, P.A. Naik, H. Singhal, J.A. Chakera, M. Kumar, M.P. Joshi, A.K. Srivastava, P.D. Gupta, Phys. Rev. A **83**, 013820 (2011)
13. Y. Pertot, L.B. Elouga Bom, V.R. Bhardwaj, T. Ozaki, Appl. Phys. Lett. **98**, 101104 (2011)
14. L.B. Elouga Bom, Y. Pertot, V.R. Bhardwaj, T. Ozaki, Opt. Express **19**, 3677 (2011)
15. M. Tudorovskaya, M. Lein, Phys. Rev. A **84**, 013430 (2011)
16. Y. Pertot, S. Chen, S.D. Khan, L.B. Elouga Bom, T. Ozaki, Z. Chang, J. Phys. B: At. Mol. Opt. Phys. **45**, 074017 (2012)
17. R.A. Ganeev, V.V. Strelkov, C. Hutchison, A. Zaïr, D. Kilbane, M.A. Khokhlova, J.P. Marangos, Phys. Rev. A **85**, 023832 (2012)
18. S. Haessler, L.B. Elouga Bom, O. Gobert, J.F. Hergott, F. Lepetit, M. Perdrix, B. Carré, T. Ozaki, P. Salières, J. Phys. B: At. Mol. Opt. Phys. **45**, 074012 (2012)
19. S. Haessler, V. Strelkov, L.B. Elouga Bom, M. Khokhlova, O. Gobert, J.F. Hergott, F. Lepetit, M. Perdrix, T. Ozaki, P. Salières, New J. Phys. **15**, 013051 (2013)
20. M. Kumar, H. Singhal, J.A. Chakera, P.A. Naik, R.A. Khan, P.D. Gupta, J. Appl. Phys. **114**, 033112 (2013)
21. H. Singhal, P.A. Naik, M. Kumar, J.A. Chakera, P.D. Gupta, J. Appl. Phys. **115**, 033104 (2014)
22. N. Rosenthal, G. Marcus, Phys. Rev. Lett. **115**, 133901 (2015)
23. M.A. Fareed, N. Thiré, S. Mondal, B.E. Schmidt, F. Légaré, T. Ozaki, Appl. Phys. Lett. **108**, 124104 (2016)
24. M.A. Fareed, S. Mondal, Y. Pertot, T. Ozaki, J. Phys. B: At. Mol. Opt. Phys. **49**, 035604 (2016)
25. M.A. Fareed, V.V. Strelkov, N. Thiré, S. Mondal, B.E. Schmidt, F. Légaré, T. Ozaki, Nat. Commun. **8**, 16061 (2017)
26. M. Wöstmann, L. Splitthoff, H. Zacharias, Opt. Express **26**, 14524 (2018)
27. Z. Abdelrahman, M.A. Khohlova, D.J. Walke, T. Witting, A. Zair, V.V. Strelkov, J.P. Marangos, J.W.G. Tisch, Opt. Express **26**, 15745 (2018)
28. M.A. Fareed, V.V. Strelkov, M. Singh, N. Thiré, S. Mondal, B.E. Schmidt, F. Légaré, T. Ozaki, Phys. Rev. Lett. **121**, 023201 (2018)
29. I.S. Wahyutama, T. Sato, K.L. Ishikawa, Phys. Rev. A **99**, 063420 (2019)
30. M. Kumar, H. Singhal, J.A. Chakera, J. Appl. Phys. **125**, 155902 (2019)
31. M.Oujja, A. Benítez-Canete, M. Sanz, I. Lopez-Quintas, M. Martín, R. de Nalda, M. Castillejo, Appl. Surf. Sci. **336**, 53 (2015)
32. S.A. Akhmanov, I.M. Bayanov, S.V. Gaponov, V.M. Gordienko, M.S. Dzhidzhoev, V.V. Ivanov, S.V. Krayushkin, S.A. Magnitsky, V.T. Platonenko, Y.Y. Platonov, Y.V. Ponomarev, A.B. Savel'ev, N.N. Salastchenko, E.V. Slobodchikov, A.P. Tarasevich, Bull. Russ. Acad. Sci. Phys. **56**, 1372 (1992)
33. M.S. Dzhidzhoev, V.M. Gordienko, V.V. Kolchin, S.A. Magnitsky, V.T. Platonenko, A.B. Savel'ev, A.P. Tarasevitch, J. Opt. Soc. Am. B **13**, 193 (1996)
34. G. Arai, H. Hara, T. Hatano, T. Ejima, W. Jiang, H. Ohashi, S. Namba, A. Sunahara, A. Sasaki, M. Nishikino, G. O'Sullivan, T. Higashiguchi, Opt. Express **26**, 27748 (2018)
35. J. Osterholz, F. Brandl, T. Fischer, D. Hemmers, M. Cerchez, G. Pretzler, O. Willi, S.J. Rose, Phys. Rev. Lett. **96,** 085002 (2006)
36. H. Kondo, T. Tomie, H. Shimizu, Appl. Phys. Lett. **72**, 2668 (1998)
37. R. Ganeev, M. Suzuki, M. Baba, H. Kuroda, T. Ozaki, Opt. Lett. **30**, 768 (2005)
38. Y. Akiyama, K. Midorikawa, Y. Matsunawa, Y. Nagata, M. Obara, H. Tashiro, K. Toyoda, Phys. Rev. Lett. **69**, 2176 (1992)
39. W. Theobald, C. Wülker, F.R. Schäfer, B.N. Chichkov, Opt. Commun. **120**, 177 (1995)
40. H.M. Milchberg, S.J. Mcnaught, E. Parra, Phys. Rev. E **64**, 056402 (2001)

41. V.P. Krainov, M.B. Smirnov, Phys. Rep. **370**, 237 (2002)
42. M. Kumar, R. Singh, U. Verma, Laser Part. Beams **32**, 9 (2014)
43. R.A. Ganeev, M. Baba, M. Suzuki, H. Kuroda, J. Appl. Phys. **99**, 103303 (2006)
44. R.A. Ganeev, M. Suzuki, M. Baba, H. Kuroda, Eur. Phys. J. D **37**, 255 (2006)
45. A.M. Rubenchik, M.D. Feit, M.D. Perry, J.T. Larsen, Appl. Surf. Sci. **129**, 193 (1998)
46. L.B. Elouga Bom, J.C. Kieffer, R.A. Ganeev, M. Suzuki, H. Kuroda, T. Ozaki, Phys. Rev. A **75**, 033804 (2007)
47. R.A. Ganeev, C. Hutchison, T. Witting, F. Frank, W.A. Okell, A. Zaïr, S. Weber, P.V. Redkin, D.Y. Lei, T. Roschuk, S.A. Maier, I. López-Quintás, M. Martín, M. Castillejo, J.W.G. Tisch, J.P. Marangos, J. Phys. B: At. Mol. Opt. Phys. **45**, 165402 (2012)
48. J. Roth, F. Géahler, H.R. Trebin, Int. J. Mod. Phys. C **11**, 317 (2000)
49. M. Wöstmann, P.V. Redkin, J. Zheng, H. Witte, R.A. Ganeev, H. Zacharias, Appl. Phys. B **120**, 17 (2015)
50. R.A. Ganeev, J. Zheng, M. Wöstmann, H. Witte, P.V. Redkin, H. Zacharias, Eur. Phys. J. D **68**, 325 (2014)
51. R.A. Ganeev, M. Suzuki, H. Kuroda, Phys. Rev. A **89**, 033821 (2014)
52. R.A. Ganeev, V. Tosa, K. Kovács, M. Suzuki, S. Yoneya, H. Kuroda, Phys. Rev. A **91**, 043823 (2015)
53. V.V. Strelkov, R.A. Ganeev, Opt. Express **25**, 21068 (2017)
54. M. Wöstmann, L. Splitthoff, H. Zacharias, Opt. Express **26**, 14524 (2018)
55. J. Seres, V.S. Yakovlev, E. Seres, C.H. Streli, P. Wobrauschek, C.H. Spielmann, F. Krausz, Nat. Phys. **3**, 878 (2007)
56. A. Pirri, C. Corsi, M. Bellini, Phys. Rev. A **78**, 011801 (2008)
57. V. Tosa, V.S. Yakovlev, F. Krausz, New J. Phys. **10**, 025016 (2008)
58. T. Fok, Ł. Wegrzyński, M. Kozlova, J. Nejdl, P.W. Wachulak, R. Jarocki, A. Bartnik, H. Fiedorovicz, Photonics Lett. Pol. **6**, 14 (2014)
59. M. Negro, C. Vozzi, K. Kovacs, C. Altucci, R. Velotta, F. Frassetto, L. Poletto, P. Villoresi, S. De Silvestri, V. Tosa, Laser Phys. Lett. **8**, 875 (2011)
60. E. Takahashi, P. Lan, O.D. Mücke, Y. Nabekawa, K. Midorikawa, Nat. Commun. **4**, 2691 (2013)
61. M. Oujja, I. Lopez Quintas, A. Benítez Cañete, R. de Nalda, M. Castillejo, Appl. Surf. Sci. **392**, 572 (2017)
62. M. Oujja, J.G. Izquierdo, L. Banares, R. de Nalda, M. Castillejo, Phys. Chem. Chem. Phys. **20**, 16956 (2018)
63. R.A. Ganeev, T. Witting, C. Hutchison, F. Frank, P.V. Redkin, W.A. Okell, D.Y. Lei, T. Roschuk, S.A. Maier, J.P. Marangos, J.W.G. Tisch, Phys. Rev. A **85**, 015807 (2012)
64. R.A. Ganeev, Phys. Usp. **58**, 772 (2013)